

EFFECT OF ECCENTRICITY ON RADIAL FORCE AND CAVITATION CHARACTERISTICS IN THE REACTOR COOLANT PUMP

by

Yuanyuan ZHAO, Xiuli WANG*, and Rongsheng ZHU

National Research Center of Pumps, Jiangsu University, Zhenjiang, Jiangsu, China

Original scientific paper

<https://doi.org/10.2298/TSCI200608312Z>

Nuclear reactor coolant pump as one of the most critical equipment is the only one rotating equipment in first loop system of nuclear power plant. Due to the asymmetric structure of the pump body, especially the existence of outlet segment lead to a certain of radial force, the magnitude of radial force directly affects the work stability of the reactor coolant pump. The nuclear reactor coolant pump could stability work under those transient complex conditions is an important index of its performance. To study the cavitation characteristics and radial force of reactor coolant pump on transient cavitation, a prototype pump and those exhibiting different gravity center offsets are analyzed numerically with CFD software ANSYS CFX by employing RNG $k-\epsilon$ model and two-fluid two-phase flow model. Through the experiment-combined simulation, the variations of cavitation characteristics and radial force of the reactor coolant pump under different eccentricities are characterized. As revealed from the results, the flow characteristics of the internal flow field of the nuclear main pump change after the axis is offset by different distance. The influence of eccentricity on the cavitation of the nuclear main pump is mainly manifested at the impeller inlet from cavitation inception severe cavitation. When the eccentricity is 5 mm, the cavitation performance is improved. The effect of eccentricity on the radial force of impeller is reflected in the variation of force direction. Compared with other plans, the radial force is superior in transient cavitation under the eccentricity of 5 mm.

Key words: reactor coolant pump, eccentricity, cavitation, radial force, numerical simulation

Introduction

The reactor coolant pump refers to the only rotating equipment in the first loop system of the nuclear power plant; it acts as critical nuclear power equipment as well. Unlike the normal centrifugal pumps, the reactor coolant pump is composed of an annular chamber with guide vane, designed to consider the stability and safety of its operation. The radial force acting on the impeller in the normal operation under the design conditions should be ensured as the minimum. Thus, the shaft is subjected to the minimum of alternating stress and directional deflection, while safe and reliable operation is ensured under high temperature, high pressure and high load. In theory, no radial force is identified in the annular chamber. In practice, however, for the presence of the outlet, the pump body exhibits an asymmetric structure, thereby generating radial force. Moreover, a large radial force will be generated in the operation of the nuclear pump when it operates under partial working conditions.

* Corresponding author, e-mail: jsuwxl@163.com

Under the transient condition of the nuclear power plant, cavitation is likely to be present in the pump. Cavitation can increase the noise and cause the vibration of the pump during pump operation. Besides, it is capable of disrupting the continuity of the flow, enhancing the resistance of the flow path and even blocking the flow path. Furthermore, serious cavitation may occur in other accidents, so the blades and stator in the pump undergo cavitation damage, which significantly reduces the safety of the nuclear power plant. Accordingly, studying the radial force of the reactor coolant pump, especially the radial force under the cavitation condition, is critical to ensure the safe and reliable operation of reactor coolant pump.

Existing studies on flow characteristics and radial force of pump under cavitation worldwide are summarized as follows. Zhu *et al.* [1] delved into the problem of cavitation under the accident of CAP1400 nuclear reactor coolant pump and characterized the complete characteristics of the reactor coolant pump under the gas-liquid two-phase flow. Zhang *et al.* [2] determined the critical pressure and critical temperature of the nuclear reactor coolant pump cavitation with CFD. Wang *et al.* [3] conducted CFD analysis of the hydrodynamic characteristics during the transition of the reactor coolant pump cavitation, and obtained the characteristics of the pressure pulsation and head fluctuation in the reactor coolant pump. Shi *et al.* [4] analyzed the effect of gap on pressure pulsation and radial force of centrifugal pumps. Wang *et al.* [5] studied the effect of eccentricity on the flow inside the nuclear main pump, and analyzed the effect of eccentricity on the radial force under the single-phase working condition. Barrio *et al.* [6] studied the radial force characteristics at the tongue of the centrifugal pump exhibiting different impeller-tongue gaps as controlled by the alteration of the impeller diameter. Gonzalez *et al.* [7] explored the capability of a numerical simulation in acquiring the dynamic and unsteady flow effects inside a centrifugal pump as impacted by the impeller-volute interaction. Moreover, they conducted the experimental and numerical studies on the steady and unsteady radial forces generated in a single volute vaneless centrifugal pump. By altering inlet pressure, flow rate and temperature of fluid, Wang *et al.* [8] determined the critical cavitation and subsequently delved into the reactor coolant pump cavitation. Franz *et al.* [9] studied the effect of cavitation on the radial forces and hydrodynamic stiffness of a centrifugal pump. Uchida *et al.* [10] measured the radial force of a centrifugal pump with a pump that was equipped with a device to measure the radial force and a volute casing with an interchangeable tongue. They also investigated the effect of cavitation on the radial force. By experimental and numerical studies, Cao *et al.* [11] clarified the effect of the impeller eccentricity on the performance of centrifugal pump. Rau *et al.* [12] analyzed the effects of different tongue clearances on pressure in fluctuation and radial force characteristics by regulating impeller and the clearance rate of 23.2-8.8%. Alqutub *et al.* [13], investigated experimentally the effects of the radial gap and flow rate on pressure fluctuations, vibration, and pump performance for two different impeller designs. Gonzalez *et al.* [14] presented experimental and numerical studies on the steady and unsteady radial forces generated in a single volute vaneless centrifugal pump. Besides, two impellers equipped with different outlet diameters were examined for the identical volute. D'Agostino *et al.* [15] investigated the linearized dynamics of the rotor dynamic forces exerted by the fluid on the rotor in whirling and cavitation radial impellers with thin logarithmic blades and under constant eccentricity and whirl speed. Lei *et al.* [16] expounded the unsteady cavitation flows in a centrifugal pump operating under off-design conditions and demonstrated the evolution of cavitation structure inside the impeller with CFD.

According to the mentioned studies, the existing research primarily focused on pump cavitation, eccentric operation and radial force. However, it does not involve the research about the effect of eccentricity on the development of cavitation and the radial force of impeller in

cavitation transition. To analyze the effect of eccentricity on the cavitation and radial force of the reactor coolant pump in cavitation transition, based on existing studies on the reactor coolant pump, the unsteady numerical simulation of cavitation transition process was performed with ANSYS CFX software after eccentric design. This study revealed the variations of cavitation characteristics and radial force of the reactor coolant pump under different eccentricities.

Methodology

Eccentricity design plan

The AP1000 nuclear reactor coolant pump was adopted in this work, the transmission medium of which was water: designed flow Q : 17886 m³/h, designed head H : 111.3 m, rotational speed, n : 1480 rpm, specific speed, n_s : 351.4. To study radial force due to asymmetric volute or partial operation, this study analyzed the effect of different angles and eccentric distances on the radial force of the reactor coolant pump under the constant geometric parameters of the pump hydraulic components, and then the center of the impeller and the guide vane that offset a certain distance toward the outlet. In fig. 1(a) is the 3-D water body diagram of the nuclear main pump, and fig. 1(b) is the schematic diagram from the Z-direction, five schemes where equally divided on the central cross-section in the range of 100° near the outlet, with 5 mm and 15 mm offsets in each direction. Subsequently, the numerical simulation was conducted. As revealed from the results, Scheme 3 significantly impacted the radial force of the reactor coolant pump. Lastly, the Scheme 3 was determined as the final eccentricity scheme. The optimal scheme was deviated by 0 mm, 5 mm, 10 mm, 15 mm, and 20 mm along the central axis. Next, the internal flow characteristics of the reactor coolant pump under the five schemes were analyzed, respectively.

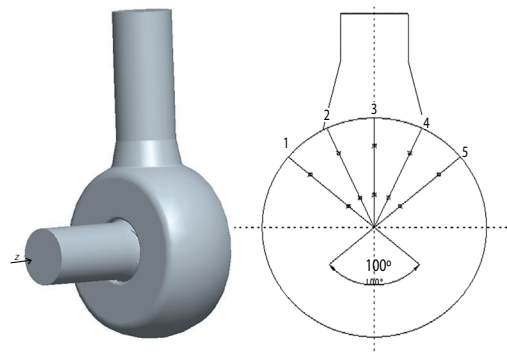


Figure 1. The 3-D model and schematic diagram of each eccentricity scheme; (a) 3-D model (b) eccentricity schemes

Calculation model and meshing

The 3-D model for calculation is generated based on PRO/E software. The whole calculation area consists of water inlet, impeller, volute and water outlet. In the present study, the structured meshes were adopted to disperse the fluid regions, as generated by the mesh generation software ICEM-CFD. Though it takes more time to generate structured meshes, it can more effectively ensure the quality of mesh generation. Moreover, it ensures the boundary-layer mesh, so the numerical simulation exhibits high convergence precision and short convergence time. Figure 2(a) illustrates the mesh discretization of the calculation area.

In theory, with the increase in the number of model meshes, the solution error attributed to the mesh tends to decrease until it is acceptable, the CFD results are not associated with the number of meshes. However, given the computer hardware configuration and calculation time, the number of the meshes should not be overly large. Given the fact of this study, to verify the mesh independence, six schemes exhibiting different mesh numbers were applied for CFD under design conditions. Moreover, the results are shown in fig 2(b). Figure 2(b) suggests that with the increase in the number of meshes, the numerical fluctuation of head tends to decrease. Under the overall grid number over $0.4 \cdot 10^7$, the head fluctuation of the two schemes is less than

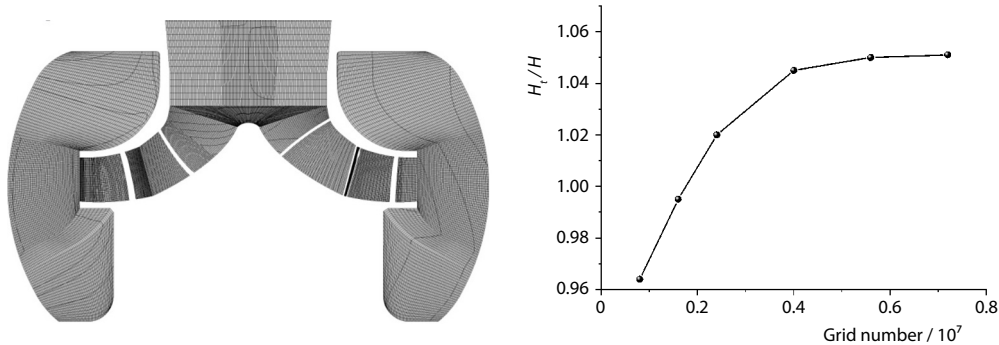


Figure 2. Grid generation and independence verification; (a) grid generation and (b) the analysis grid independence

0.1%, which is considered to support the mesh-independent assumption. Given the time and accuracy of numerical simulation, the meshing scheme was finally determined for subsequent research. Table 1 shows the final mesh number plan of reactor coolant pump.

Table 1. Meshing of reactor coolant pump

Component	Inlet	Impeller	Stator	Volute	Outlet	Total
Number	417653	1812832	1068505	2028715	353262	5680967

Numerical calculation methods and boundary conditions

The ANSYS CFX 14.0 software was employed for the steady calculation of cavitation and determined the cavitation inception working condition of the reactor coolant pump. With the initial condition of the steady calculation of the cavitation inception, the RNG $k-\varepsilon$ turbulence model and two-fluid two-phase flow model were adopted to conduct the unsteady calculation since the RNG $k-\varepsilon$ turbulence model is capable of simulating the high strain effectively in calculating rotational flow. The interface in unsteady calculation was set as Transient Rotor-Stator mode. The unsteady numerical simulation time step was $3.378 \cdot 10^{-3}$ second, and the total calculation time was 0.3649 second. To ensure the accuracy of the numerical calculation results, the impeller rotated one revolution based on the stable results, and then it conducted the calculation for cavitation transition.

To study the characteristics of cavitation and radial force in the transition of the reactor coolant pump, the linear changes of inlet pressure were analyzed in this article. The CFX cel set changes of inlet pressure were used, and the function is defined:

$$p(t) = \begin{cases} p_a & t < 0.04054 s \\ p_a + p_0(t - t_0) & t > 0.04054 s \end{cases} \quad (1)$$

where $p(t)$ [Pa] is the inlet pressure, p_a [Pa] – the inlet pressure at the critical cavitation of the reactor coolant pump, p_0 – the pressure coefficient, t [s] – the time, and t_0 – the initial time, 0.04054 second.

Under the outlet conditions (*e. g.*, the outlet mass-flow), the flow of the calculated model was controlled by the outlet boundary conditions. Standard wall functions were selected near the wall. The wall boundary condition was set as the adiabatic non-slip wall. The average bubble diameter was set to $2 \cdot 10^{-6}$ m. The volume fraction of water at the inlet was set to 1, and the volume fraction of the bubble was set to 0. The computational convergence accuracy was 10^{-5} .

Simulation analysis and discussion

Definition of the reactor coolant pump cavitation on each stage

The test data is consistent with the numerical simulation data. The head changes over time of the reactor coolant pump under the eccentricity $e = 0$. As revealed from the results, the process of cavitation inside the reactor coolant pump impeller is similar under each eccentricity scheme. Accordingly, the stages of cavitation were defined by the scheme of eccentricity $e = 0$.

The initial working condition of unsteady calculation was the cavitation inception working condition of the reactor coolant pump. The head was reduced by nearly 3% at $t = 0.29$ seconds, and the initial time to 0.29 seconds was defined as the stage of cavitation inception the critical cavitation. At $t > 0.29$ seconds, the head descending trend was accelerated; note that after 0.34 seconds, it began to exhibit fracture decline. $0.29 < t < 0.3649$ seconds was defined as the stage of serious cavitation and fracture cavitation.

Holistic cavitation characteristics in impeller under fracture cavitation

Figure 3 gives a graph of the total gas volume fraction in the impeller during fracture cavitation in which fig. 3(b) is a partial enlarged view of $0.32 < t < 0.36$ seconds in fig. 3(a). The three dashed lines in fig. 3(a) are tangent to the curve of the total gas volume fraction in the impeller at three different periods. The slope of the three tangent curves indicates the rate of increase of the volume fraction of the whole gas at different periods. As the cavitation progresses to the fracture cavitation, the rate of increase of the volume fraction of the whole vapor phase displays a slight elevation with the deepening of the cavitation. The mentioned finding is probably because when the reactor coolant pump is in serious cavitation, the cavitation near the impeller entrance stops developing. Cavitation will develop with the flow of the liquid to the downstream of the impeller flow passage, and the large bubble accumulation area will be expanded. The difference between the curves in each group in fig. 3 is also smaller than that of the single monitoring point. It is therefore, revealed that the regularity of the cavitation characteristics of the reactor coolant pump is overall stable, while the large local differences do not alter the overall development of cavitation regulation.

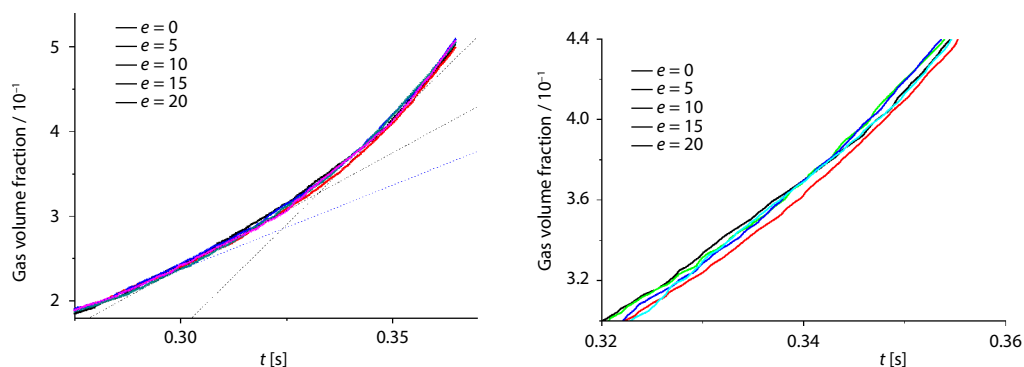


Figure 3. The overall and partial enlarged graphs of the total gas volume fraction in the impeller during fracture cavitation; (a) the overall graph of the total gas volume fraction in the impeller during fracture cavitation and (b) partial enlarged graph of $0.32 < t < 0.36$ seconds

As suggested in fig. 3(b), and the cavitation performance of each scheme is ranked as $e = 5 > e = 20 > e = 15, e = 10$ and $e = 0$ within $0.275 < t < 0.34$ seconds. With the deepening of the cavitation in the impeller, the differences of the schemes decrease. At $t = 0.34$ seconds, except the $e = 0$ scheme, the other four curves intersect, and the eccentricity exerts the minimum effect on the cavitation characteristics of the reactor coolant pump. After $t > 0.34$ seconds, as revealed from the results, the cavitation performance of each scheme was ranked as $e = 5 > e = 20, e = 0 > e = 10, e = 15$. Compared with the previous stage, the cavitation characteristics change. With the development of the degree of cavitation, differences between the various schemes increase. In fig. 3(a), the curves reveal that in the development of serious cavitation fracture cavitation, the ratio of the total volume of gas in impeller reaches the minimum in respective scheme under the eccentricity $e = 5$. Thus, it is known that the cavitation performance of $e = 5$ eccentricity scheme is improved. At the fracture cavitation stage, the volume fraction of the vapor phase reaches 40%–50%. Then, considerable bubbles will block the normal delivery of the coolant and adversely affect the safe operation of the reactor coolant pump in an extreme manner.

The overall variation regulation of radial forces of each eccentricity scheme

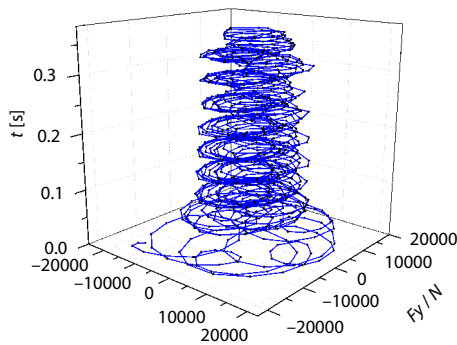


Figure 4. The time-domain diagram of radial forces distribution for the eccentricity scheme $e = 5$

Figure 4 presents the time-domain diagram of radial forces distribution for the eccentricity scheme $e = 5$. The Z-axis is time t [s]. The curves of the diagram are clearly divided into nine independent phases along the Z-axis, complying with nine turns of the impeller in the entire numerical calculation. In fig. 4, the impeller radial forces of each turns exhibit a consistent variation regulation. As revealed from the comparison of each figure, the radial forces varies gently from the cavitation inception the serious cavitation, demonstrating that the reactor coolant pump impeller is subjected to cyclical radial forces during rotation, and the variation regulation of radial forces is primarily determined by the liquid-flow characteristics in the impeller.

The variation regulation of the resultant force of radial forces in each eccentricity scheme

Figure 5 gives a graph of the resultant force of radial forces under each eccentricity scheme, where figs. 5(b) and 5(c) are partial magnifications of the resultant force of radial forces at $0.06 < t < 0.12$ seconds and $0.30 < t < 0.36$ seconds. Figure 5 suggests that the radial forces experienced by the impellers in each eccentricity scheme vary cyclically, and the peak-trough time is nearly 0.0037 seconds. In the cavitation inception and critical cavitation stages of the reactor coolant pump, the distribution of resultant force of radial forces in the time domain displays the identical trend. The amplitude of radial force is about 12 KN, and no big fluctuation is identified in the resultant force of radial forces. Under serious cavitation and fracture cavitation conditions, the amplitude of radial force is slightly larger than that of cavitation inception and critical cavitation. The radial force amplitude is approximately 14 KN, with the development of cavitation, the amplitude of radial force increases.

As revealed from the comparison of figs. 5(b) and 5(c), when $t < 0.15$ seconds, the curves overlap. Then, each eccentricity scheme less impacts the radial force. After $t > 0.15$ seconds, the curves no longer overlap, suggesting the difference in the X - and Y -axis directions. The difference in X -axis direction appears with the peak-trough of radial forces no longer synchronized. In Y -axis direction, the difference is present as that of the resultant force magnitude of radial forces of each scheme, and it becomes obvious with the development of cavitation. As shown in fig. 5(c), the resultant of radial forces of respective eccentricity scheme at each peak of the curve varies more significantly than that at the trough at the peak. Thus, the vibration of the reactor coolant pump will aggravate and become unstable in this period. At $t = 0.30$ seconds and $t = 0.34$ seconds, the time-domain distribution of the radial force is significantly constricted. The difference of radial force is the most prominent at the two time points, and then the resultant force of radial forces rapidly increases while the difference between the curves has diminished. The difference between the two time points $t = 0.30$ seconds and $t = 0.34$ seconds is about one revolution time of the impeller. As revealed from the analysis of the radial force between the two time points, the radial force first increases and then decreases during one revolution of the impeller. According to the distribution of the radial forces in fig. 5, it is reported that the direction of radial forces fluctuates obviously after $t > 0.3$ seconds, demonstrating that the eccentricity affects the cavitation state of the reactor coolant pump primarily in the variation of the radial force in the severe and fracture cavitation stage.

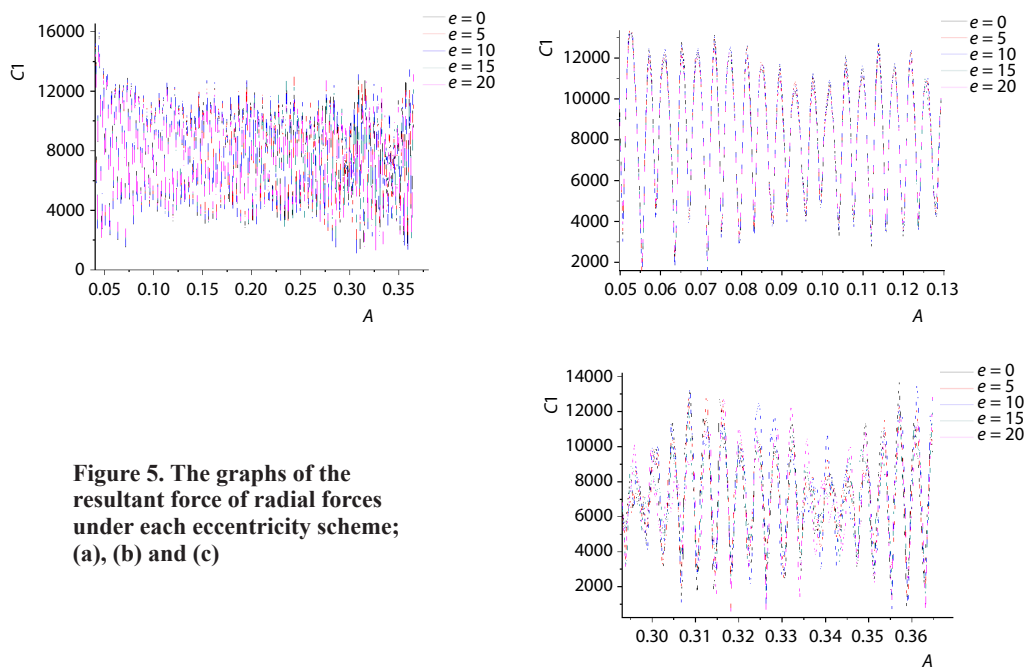


Figure 5. The graphs of the resultant force of radial forces under each eccentricity scheme; (a), (b) and (c)

Radial force variation under fracture cavitation of each eccentricity scheme

Figures 6(a)-6(e) gives the time-domain diagram of the radial force under fracture cavitation of each eccentricity scheme. When the reactor coolant pump is in fracture cavitation condition, the corresponding radial force is affected by considerable bubbles accumulated in

the impeller, and the magnitude and direction of radial force are greatly fluctuated. The radial force varies gently from cavitation inception serious cavitation, revealing that the bubble has little effect on the radial force before the bubble spreads to the entire impeller runner. Each rotation of the reactor coolant pump impeller will make the radial force rotate 11 cycles, *i.e.*, the impeller will undergo 11 periodic radial forces during one rotation. The direction of the radial force rotates counterclockwise, and the impeller rotates 32.7° each circle of radial force. The mentioned periodic variation is impacted by the static and dynamic interference between the guide vane and the impeller.

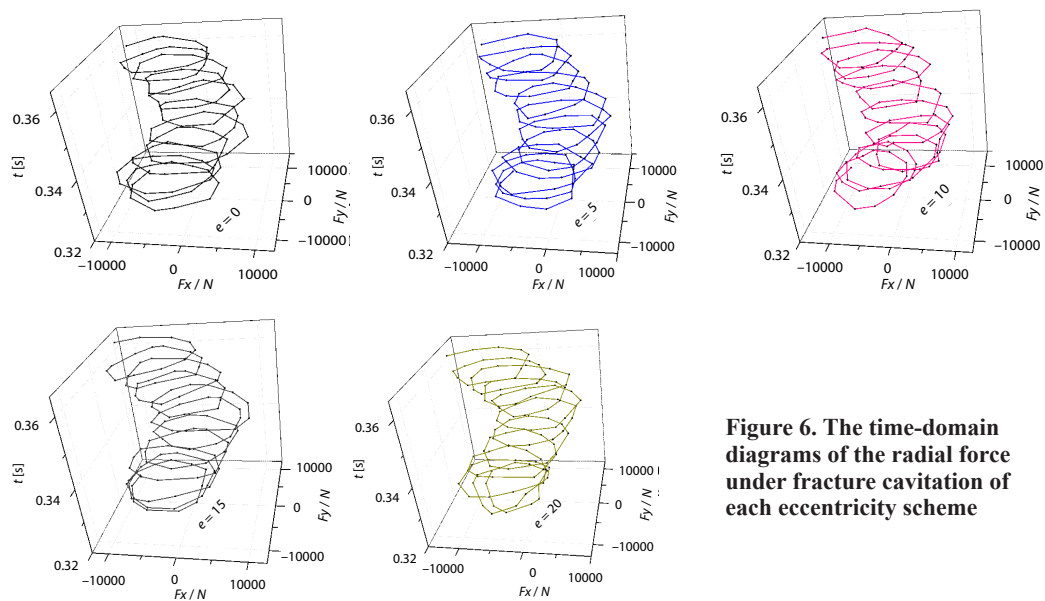


Figure 6. The time-domain diagrams of the radial force under fracture cavitation of each eccentricity scheme

Figure 6 suggests that under the eccentricity $e = 0$, the radial force first moves in the $+X$ -axis direction; the radial force will shift to the $-X$ -axis direction and move to the original position after the impeller rotates for half a turn. The radial force distribution center is obviously biased toward the $-X$ -direction, complying with the eccentricity $e = 15$ scheme. In the eccentricity $e = 5$ scheme, the radial force returns to its original position after moving along the X -axis. Under this eccentricity scheme, the center of radial force distribution of the reactor coolant pump is approximately in the identical position at different stages of cavitation. Under the eccentricity $e = 10$, the center of radial force distribution is unclear. Its movement follows the X -direction but slightly deviates. As a result, the radial force primarily distributes in the second and the fourth quadrant under the eccentricity $e = 10$. In the eccentricity $e = 20$ scheme, radial force primarily along the $+X$ angle of 45° to do the reciprocating movement. After one rotation of the impeller, the radial force moves to the original position. The distribution of radial force at the same angle of the impellers is similar, demonstrating that under the small eccentricity, the radial force distribution of the reactor coolant pump primarily determined by the matching relationship between the impeller and other overflow components. As the eccentricity increases, the effect of eccentricity on the radial force distribution of the reactor coolant pump increases, changing the original law of radial force reciprocating along X .

As revealed from the comparison of fig. 6 with each figure, the radial force of the reactor coolant pump impeller at fracture cavitation vary differently under different eccentricities. In

the three schemes of eccentricity, *i.e.*, $e = 0$, $e = 5$, and $e = 15$, the radial forces rotate about 32.7° counterclockwise with each rotation of the impeller at 3° , and the direction varies uniformly with no significant variation. In the eccentricity schemes $e = 10$, $e = 20$, the direction of radial force varies dramatically, and with the impeller cavitation further develops, the variation in the direction of radial force becomes messier.

Experimental verification

To verify the accuracy of the simulation result of the reactor coolant pump, the design parameters of the reactor coolant pump were reduced in a certain proportion. The model pump was produced according to the reduced proportion. Then, it was employed for experimental verification. The test rig of the reactor coolant model pump is illustrated in fig. 7. According to the experimental data obtained from the model pump, the similar conversion method was adopted to calculate the data consistent with the prototype pump. Compared with the results of the CFD simulation calculation, it is considered that the efficiency remains unchanged before and after conversion.



Figure 7. The diagram of test site

Where Q denotes the flow of prototype pump, with Q_M [m^3h^{-1}] as that of the model pump, H is the head of prototype pump, with H_M [m] as that of the model pump, P indicates the power of prototype pump, with P_M [kW] as that of the model pump, D is the diameter of prototype pump, with D_M [mm] as that of the model pump, n is the rotational speed of prototype pump, with n_M [rpm] as that of the model pump.

The performance curve can be converted by the aforementioned formula. The experimental equipment employed in the experiment included turbine flowmeter, vacuum pump, electric parameter measuring instrument, pressure sensor, pump parameter comprehensive tester, DC resistance tester, regulating valve, pressure system console, as well as distribution system for motor starting.

The contrast results are present in fig. 8. In fig. 8, the abscissa refers to the ratio of the flow rate Q to the designed flow rate $Q_b = 17886 \text{ m}^3/\text{h}$. The left vertical co-ordinate represents the head H , and the right vertical co-ordinate indicates the efficiency η . The figure suggests that the variations of experimental and simulation values are nearly identical, and the experimental value is smaller than the simulation one. The mentioned finding is because when doing numerical simulation for prediction, only the hydraulic efficiency of the fluid calculation domain is considered without the leakage and mechanical losses, so the predicted value reaches over the actual experimental value of the model pump.

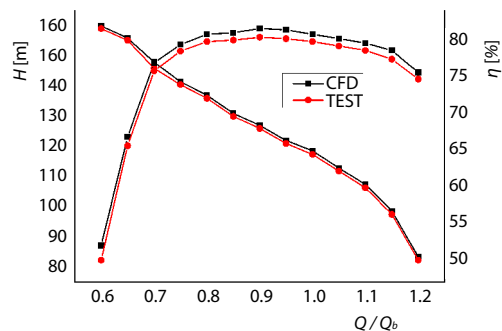


Figure 8. The diagram of contrast results

Accordingly, the CFD calculation results can be considered to roughly reflect the practical situation of the experiment, and the CFD calculation mentioned previously is credible.

Conclusion

- When the axis of the reactor coolant pump is shifted, the flow characteristics of the internal flow field will be altered. In the eccentricity $e = 5$ scheme, the cavitation performance of the reactor coolant pump is optimized, and the radial force distribution tends to be reasonable.
- The overall cavitation of the scheme with the eccentricity $e = 5$ outperforms that of other schemes. Before the serious and fracture cavitation, the radial force of the impeller varies in a gentle manner. At the severe and fracture cavitation stage, the radial force of the impeller slightly increases. The pulsation of the resultant force of radial forces is the maximum nearby the two times the blade frequency, in which the differences between the schemes are most significant. After six times the blade frequency, the pulsation tends to be gentle.
- The effect of eccentricity on the radial force of the reactor coolant pump impeller is primarily reflected in the direction of force. Under the eccentricity of 5 mm, the variation of the radial force direction is more orderly than that of other eccentricity schemes, *i.e.*, the optimal scheme.

Nomenclature

e – eccentricity, [–]	p_0 – pressure coefficient, [–]
p_a – inlet pressure at the critical cavitation, [Pa]	t – time, [s]
$p(t)$ – inlet pressure, [Pa]	t_0 – initial time, [s]

Reference

- [1] Zhu, R. S., et al., Numerical Study on Cavitation Characteristics of CAP1400 Nuclear Main Coolant Pump, *Journal of Drainage and Irrigation Machinery Engineering*, 34 (2016), 6, pp. 490-495
- [2] Zhang, Y., et al., Inception Behavior of the Cavitation in Nuclear Reactor Cooling Pump, *Journal of Engineering Thermophysics*, 31 (2010), S1, pp. S57-S60
- [3] Wang, X. L., et al., Analysis on Transient Hydrodynamic Characteristics of Cavitation Process for Reactor Coolant Pump, *Atomic Energy Science and Technology*, 48 (2014), 8, pp. 1421-1427
- [4] Shi, W. D., et al., Influence of Gap on Pressure Pulsation and Radial Force of Centrifugal Pumps, *Journal of Drainage and Irrigation Machinery Engineering*, 30 (2012), 3, pp. 260-264
- [5] Wang, P., et al., Numerical Analysis on Effects of Nuclear Main Pump Radial Force under Different Eccentricities, *Journal of Drainage and Irrigation Machinery Engineering*, 33 (2015), 6, pp. 461-466
- [6] Barrio, R., et al., Numerical Analysis of the Unsteady Flow in the Near-Tongue Region in a Volute-Type Centrifugal Pump for Different Operating Points, *Computers & Fluids*, 39 (2010), 6, pp. 859-870
- [7] Gonzalez, J., et al., Steady and Unsteady Radial Forces for a Centrifugal Pump with Impeller to Tongue Gap Variation, *Journal of Fluids Engineering*, 128 (2006), 3, pp. 454-462
- [8] Wang, W., Lu, P. B., The Cavitation Research in Reactor Coolant Pump, Power and Energy Engineering Conference (APPEEC), *Proceedings*, 2010 Asia-Pacific, IEEE, Port Dickson, Malaysia, 2010, pp. 1-4
- [9] Franz, R. J., et al., On the Effect of Cavitation on the Radial Forces and Hydrodynamic Stiffness of a Centrifugal Pump, National Aeronautics & Space Administration, Washington D.C., 1986
- [10] Uchida, N., et al., Radial Force on the Impeller of a Centrifugal Pump, *Bulletin of JSME*, 14 (2008), 76, pp. 1106-1117
- [11] Cao, W., et al., The Influence of Impeller Eccentricity on Centrifugal Pump, *Advances in Mechanical Engineering*, 9 (2007), 9, pp. 16878140-1772249
- [12] Rau, B. L., et al., The Effect of Impeller Cutback on the Fluid-Dynamic Pulsations and Load at the Blade-Passing Frequency in a Centrifugal Pump, *Journal of Fluids Engineering*, 130 (2008), 11, pp. 1349-1357
- [13] Alqutub, A., et al., Experimental Investigation of the Effect of Radial Gap and Impeller Blade Exit on Flow-Induced Vibration at the Blade-Passing Frequency in a Centrifugal Pump, *International Journal of Rotating Machinery*, 2009 (2014), 1023-621X, 9
- [14] Gonzalez, J., et al., Steady and Unsteady Radial Forces for a Centrifugal Pump with Impeller to Tongue Gap Variation, *Journal of Fluids Engineering*, 128 (2006), 3, pp. 454-462

- [15] D'Agostino, L., Venturini-Autieri, M. R., Rotordynamic Fluid Forces on Whirling and Cavitating Radial Impellers, *Proceedings, 5th International Symposium on Cavitation*, Osaka, Japan, 2003, pp. 1-5
- [16] Lei, T., *et al.*, Numerical Simulation of Unsteady Cavitation Flow in a Centrifugal Pump at Off-Design Conditions, *Proceedings, Institution of Mechanical Engineers, Part C: Journal of Mechanical Engineering Science*, 228 (2014), 11, pp. 1994-2006